



## New two-component water sorbent $\text{CaCl}_2$ -FeKIL2 for solar thermal energy storage

Alenka Ristić<sup>a,\*</sup>, Darja Maučec<sup>a</sup>, Stefan K. Henninger<sup>b</sup>, Venčeslav Kaučič<sup>a</sup>

<sup>a</sup>National Institute of Chemistry Slovenia, Hajdrihova 19, 1001 Ljubljana, Slovenia

<sup>b</sup>Fraunhofer Institute for Solar Energy Systems, Heidenhofstr. 2, 79110 Freiburg, Germany

### ARTICLE INFO

#### Article history:

Available online 14 July 2012

#### Keywords:

FeKIL2  
Composite  
 $\text{CaCl}_2$   
Water sorbent  
Solar thermal energy storage

### ABSTRACT

A new two-component (composite) water sorbent  $\text{CaCl}_2$ -FeKIL2 has been developed for sorption-based solar thermal energy storage. The matrix of the composite is FeKIL2 material with disordered mesopores, high surface area of 712  $\text{m}^2/\text{g}$  and mesopore dimensions between 4 and 29 nm. The composite, prepared by wet impregnation of FeKIL2 with  $\text{CaCl}_2$ , has lower surface area (418  $\text{m}^2/\text{g}$ ) and similar mesopore dimensions as the matrix. The maximum water sorption capacity of FeKIL2 is 0.21 g/g, while the composite possesses 3 times higher maximum water sorption capacity due to the presence of the salt in the matrix. Heat of adsorption of the composite is 50.4 kJ/mol. A short-term cycling test between temperatures of 150 and 40 °C at a water vapour pressure of 5.6 kPa confirms a comparatively good hydrothermal stability of the composite.

© 2012 Elsevier Inc. All rights reserved.

### 1. Introduction

Within the next 20 years, the supply of fossil fuels, mainly oil and natural gas, will not be sufficient anymore to meet the world's energy demand. In addition, the use of fossil energy contributes to large  $\text{CO}_2$  emissions and consecutively climatic problems including the greenhouse effect. A large share of the energy consumption is due to heating and cooling systems in the urban environment. Alternatively, renewable energy technologies can be used, of which solar is the most plentifully available, and is highly suitable for generation of heat. A problem in using solar energy for heating is the mismatch between demand and solar supply. This problem can be solved by storage of the generated heat. One of the very promising concepts of heat storage is by using sorption heat storage, which is based on a reversible physico-chemical process (mostly water adsorption on solid sorbents). This process, which is graphically presented in Fig. 1, usually consists of two phases. The first phase (A) consists of the charging / regeneration phase where heat at high temperature level is available, e.g. from a solar collector at a sunny day or waste heat, and is used for desorption of water from the sorbent. The water vapour is released and condenses at ambient conditions, whereas the sorbent remains in a dry state. The second phase (B) is the generation / discharging process itself, where water vapour is evaporated by the use of a low temperature heat source, e.g. a bore hole or again a solar collector at a cloudy day, and reacts with the dry material with release of heat at medium temperature level, which can be used for heating.

In general, thermally stable microporous and mesoporous adsorbents can be used as storage materials mostly in combination with water as working fluid for application in adsorption heat pumps and thermo-chemical heat storage [1–3]. Some demonstration storage systems for heating and cooling were tested using Zeolite 13X, Zeolite 4A and silica gel as adsorbents with water as an adsorbate [4,5]. The advantage of mesoporous ordered silicas and silica gels is their low charging temperature. Thus, these materials can be used for storage of low temperature heat (e.g. solar energy) and industrial waste heat [1]. Mesoporous disordered silicas (silica gels) are widely studied as hydrophilic compounds due to the high affinity to water vapour, large water sorption capacity at low humidity and moderate temperatures for solar thermal energy exploitation regeneration ( $\sim 150$  °C) [6,7]. On the other hand, mesoporous ordered silicas, like MCM-41 and SBA-15, exhibit adsorption characteristics different from disordered mesoporous silicas, like ordinary silica gels, and they can adsorb large amount of water due to the amorphous surface structure [8].

Hydrophilic adsorbents can be developed also by the introduction of transition metals in the porous silica matrix, which are able to change colours under humidity due to hydration of the transitional metals [6]. Tuning chemical composition during synthesis can result in different number and type of active sites and polarity of the framework.

A strategy to improve the sorption capacity is the preparation of the composite (two-component) materials by combining the advantages of hygroscopic salts (halides, sulphates and nitrates of alkali and alkali-earth metals) with those of the pure porous materials (matrix) [1,9,10–16]. Different host materials are used, mostly disordered porous silicas, ordered mesoporous silica and

\* Corresponding author. Tel.: +386 147 60 215; fax: +386 147 60 300.  
E-mail address: [alenka.ristic@ki.si](mailto:alenka.ristic@ki.si) (A. Ristić).

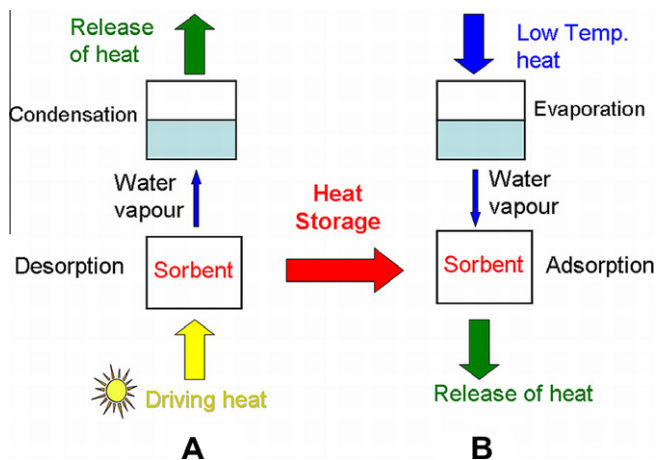


Fig. 1. Scheme of the concept of the sorption heat storage.

alumina. Besides commercially available porous oxides, natural clay, like attapulgite can also be used [17]. It is well known that the hygroscopic salts have greater water sorption capacity than the porous matrix. However, their performance decreases when equilibrium is achieved after the formation of solid crystalline hydrates [6]. A drawback of hygroscopic chlorides is the formation of solution during hydration and their corrosion. The role of the hygroscopic salt in the composites was described in detail by Aristov and co-workers [9–11,15,16], showing that the hygroscopic salt in the composite was an active component and interacted with water to increase the sorption capacity. A study of water sorption properties of the composites revealed that the formation of salt hydrates in the dispersed state happened at a lower relative pressure of water vapour with respect to the bulk state. This makes a composite containing a dispersed salt much more efficient than a common bulk salt. The influence of the porous matrix is also important, as the matrix absorbs water and serves as a dispersion medium, which forms a required salt particle size and high salt surface area. In addition this affects the state and properties of the salt, and conducts heat through the solid [9]. The main disadvantage of the composite sorbents is the corrosion and leakage of the hygroscopic salt from the mesopores, resulting in a degradation of the adsorption properties [18].

In this work, we report on the study of the structural properties of new water composite sorbent, consisting of iron silicate with disordered mesopores with KIL2 structure [19] as the matrix and salt hydrate  $\text{CaCl}_2$ . The introduction of iron into the network of KIL2 silica results in the development of more hydrophilic sorbent FeKIL2 than KIL2. Water sorption properties of the composite  $\text{CaCl}_2$ -FeKIL2 were studied in detail for low-temperature heat storage application. To design the effective composite sorbent for heat storage application, it is necessary to determine structural characteristics, which are responsible for the sorption properties of the sorbent.

## 2. Experimental

### 2.1. Synthesis

Disordered mesoporous iron silicate, named FeKIL2, with a molar ratio of Si/Fe 80 has been prepared by the modified two-step synthesis [19], where  $\text{FeCl}_3$  was used as well as the gel was solvothermally treated in a 50 ml Teflon-lined stainless steel autoclave at 150 °C for 24 h. The removal of the template was performed by the calcination at 500 °C for 10 h using a ramp rate of 2 °C  $\text{min}^{-1}$  in air. By this, the thermal stability of the product was also proven.

The principal hydrothermal stability of the products was verified by keeping the calcined sample in boiling water for 2 h [19]. Then the composite was prepared by wet impregnation of the initial FeKIL2 with 2.1 M aqueous solution of calcium chloride. After adding FeKIL2 matrix to calcium chloride aqueous solution, the mixture was stirred using a magnetic stirrer for 1 h to ensure calcium chloride penetration into the pores. The composite was filtered, washed with ethanol and dried over night at room temperature.

### 2.2. Methods

The XRD patterns were obtained on a Siemens D5000 using  $\text{CuK}\alpha$  radiation ( $\lambda = 1.5406 \text{ \AA}$ ). Samples were scanned over a range of 0.5–40°  $2\theta$  with a step of 0.04° to detect the presence of the mesostructure and of  $\text{CaCl}_2$ . Morphology of the mesoporous matrix and composite was observed using scanning electron microscopy on Zeiss Supra™ 3VP microscope. Elemental analysis of  $\text{CaCl}_2$  in the composite before and after the cycling test was performed by energy dispersive X-ray analysis (EDAX) with an INCA Energy system attached to a Zeiss Supra™ 3VP microscope. TEM micrographs were obtained on a 200-kV field-emission gun (FEG) microscope JEOL JEM 2010F. Nitrogen physisorption measurements were performed on a Tristar volumetric adsorption analyzer (Micromeritics). The BET specific surface area [20],  $S_{\text{BET}}$ , was calculated using the adsorption branch in the relative pressure range between 0.05 and 0.21. The total pore volume was estimated from the amount sorbed at a relative pressure of 0.96. The primary mesopore volume  $V_p$  and the external surface area  $S_{\text{ex}}$  were determined using the  $s$ -plot method [21] from the adsorption data in the range of the standard reduced adsorption from 2.2 to 2.6. The same method was applied to show the presence of microporosity in these materials. The micropore volume  $V_{\text{mi}}$  was estimated from the  $s$  interval from 0.75 to 1.00 [22]. In the  $s$ -plot calculations, a macroporous silica material LiChrospher Si-1000 ( $S_{\text{BET}} = 22.1 \text{ m}^2 \text{ g}^{-1}$ ) was used as a reference adsorbent [23]. The pore size distributions (PSDs) were calculated from nitrogen adsorption data using an algorithm based on theory of Barrett, Joyner, and Halenda (BJH) [24]. The maxima on the PSD are considered as the primary mesopore diameters for given samples. Thermogravimetric investigation was performed with a SDT 2960 Thermal Analyzer. For all measurements, samples were heated in a stream of nitrogen with a heating rate of 10 K/min. Prior to the TG measurements, samples were stored in a desiccator over saturated ammonium chloride solution for 7 days. Diffuse reflectance electronic spectra were measured using UV/VIS spectrophotometer Lambda 19 (Perkin-Elmer) equipped with an integrating sphere. Powder samples were loaded in a 1 mm quartz cell and spectra were collected in the wavelength range from 200 to 800 nm. Water adsorption characteristics were measured by simultaneous thermogravimetry and differential scanning calorimetry (TG–DSC 111 Setaram). The Setaram TG/DSC allows simultaneous measurement of the water uptake and the resulting heat flow. These measurements are performed under a humidified carrier gas (Argon 5.0, purity 99.999%). The experimental setup and the corresponding error analysis are described in detail elsewhere [25]. The chosen operating conditions were the following: a maximum desorption temperature of 150 °C and a minimum adsorption temperature of 40 °C or 20 °C for water vapour pressures of 5.6 and 1.2 kPa, respectively. The heat of adsorption and the integral cycle heat including the heat capacity of the material itself were determined using the following procedure: the samples were dried at 150 °C for 10 h at 0% relative humidity (RH) in a continuous argon gas flow; the relative humidity was increased to 16.3% under isothermal conditions (150 °C) for another 6 h; the heat of adsorption at 40 °C was evaluated in an isothermal humidity step; and, finally, the sample was isobarically heated to 150 °C and then cooled to 40 °C for a relative

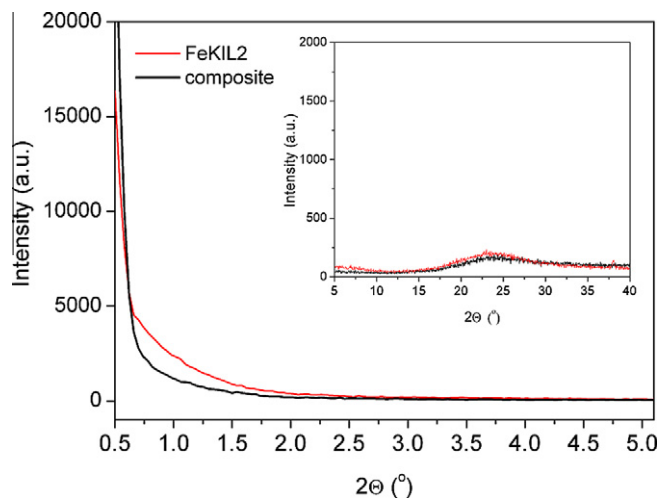


**Fig. 2.** Low-angle and high-angle (Inset) XRD patterns of the mesoporous FeKIL2 and the composite  $\text{CaCl}_2$ -FeKIL2.

humidity of 75.8%, leading to the integral heat of adsorption,  $Q_{\text{int}}$ , for the heat transformation cycle. To evaluate the hydrothermal stability of the materials, the samples have been exposed to a short-cycle hydrothermal treatment consisting of 20 cycles between temperatures of 150 and 40 °C at a water vapour pressure of 5.6 kPa. The water uptake for each cycle between 150 and 40 °C has been determined as a first benchmark.

### 3. Results and discussion

#### 3.1. Structural characterization

The powder XRD patterns shown in Fig. 2 indicate the disordered mesostructure of FeKIL2 [19] and of the composite. High-angle powder XRD (Inset of Fig. 2) was employed to detect the presence of calcium chloride in the composite. Elemental analysis showed that the composite contained 7 wt.% of  $\text{CaCl}_2$ . No diffraction peaks corresponding to  $\text{CaCl}_2$  are observed in this XRD pattern. This could be explained with the presence of highly dispersed  $\text{CaCl}_2$  with nanosized dimensions that are not detectable by XRD technique and are located on the surface and within the mesopores. The high-angle XRD pattern shows only one broad peak at a  $2\theta$  23° corresponding to glass-like amorphous FeKIL2 particles [19].

TEM images of FeKIL2 and of the composite (Fig. 3A and B) reveal that these materials are composed of amorphous iron silicate nanoparticles and many interparticle pores (textural porosity) with a very broad range of dimensions (4–29 nm).

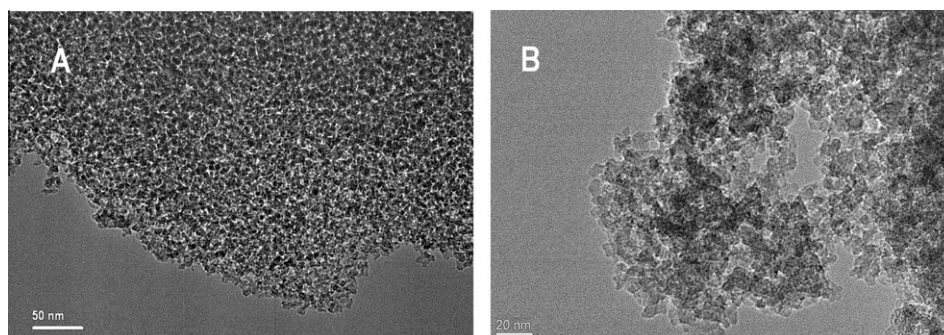


**Fig. 3.** TEM pictures (A) of the disordered mesoporous FeKIL2 and (B) of the composite  $\text{CaCl}_2$ -FeKIL2.

Porous structure of FeKIL2 and the composite was also studied by nitrogen adsorption isotherms. Nitrogen adsorption isotherms for FeKIL2 and  $\text{CaCl}_2$ -FeKIL2 are shown in Fig. 4A, whereas structural parameters determined on the basis of these isotherms are listed in Table 1. FeKIL2 sample exhibits adsorption isotherm typical for KIL2 silica [19]. The adsorption and desorption branches are almost vertical and nearly parallel, indicating on the material with pores filling and emptying in a narrow pressure range. It can clearly be observed that the presence of  $\text{CaCl}_2$  in the FeKIL2 support leads to a significant change in the shape of the hysteresis loop. The hysteresis loop of this sample is less intense and is closing down at lower  $p/p_0$  values in comparison to the original matrix, which indicates that the pores are partially narrowed with  $\text{CaCl}_2$  nanoparticles. The presence of the dispersed  $\text{CaCl}_2$  nanoparticles on FeKIL2 not only led to a decreased mesopore volume (from 1.656 to 1.286  $\text{cm}^3 \text{g}^{-1}$ ), but also resulted in an appreciable tailing of the hysteresis loop, thus evidencing the formation of material with plugs of  $\text{CaCl}_2$  in pores [26–29]. An additional difference in the nitrogen isotherm of the composite is evident. Namely, desorption branch of the composite isotherm is divided in two steps. The first step is similar to desorption in pure FeKIL2 due to desorption of  $\text{N}_2$  from the open pores; the second desorption step can be attributed to the  $\text{CaCl}_2$  nanoparticles (plugs) within the mesopores (the narrowed mesopores) [29]. Therefore, it can be concluded that  $\text{CaCl}_2$  nanoparticles have been dispersed inside the pores of FeKIL2.  $\text{CaCl}_2$  is also present on the external surface of the composite. This evidence is clearly seen in relative pressure range from 0.95 and 1, where the hysteresis loop due to textural porosity becomes smaller.

Pore size distribution of the different mesoporous materials has been determined using the BJH model widely used for this type of samples [30]. Although this model often underestimates pore sizes [31], it is appropriate for comparative purposes. Fig. 4B displays the pore size distributions determined from adsorption isotherms. It is clear that after impregnation two maxima appear representing the open mesopores and the narrowed mesopores, while pore size distribution of FeKIL2 shows only one maximum (17.6 nm). As it can be observed, the maximum of the open mesopores of the composite shifts to higher pore size (17.9 nm) [30], while the maximum characteristic for narrowed mesopores shifts to lower pore diameter (11.7 nm).

Diffuse reflectance UV–Vis spectroscopy was used to investigate the nature of the ferric ion in FeKIL2. UV–Vis spectra of Fe-containing zeolites are characterized by intense  $\text{Fe}^{3+} \rightarrow \text{O}$  charge-transfer (CT) bands, the position of which provided information on the coordination and degree of agglomeration [32]. Thus, isolated  $\text{Fe}^{3+}$  ions give rise to bands below 300 nm, while signals of small oligonuclear  $\text{Fe}_x\text{O}_y$  clusters within the pores appear between 300 and 400 nm and  $\text{Fe}_2\text{O}_3$  nanoparticles at the external surface of the crystal above 400 nm [33]. Usually, two CT transitions are observed for more or less distorted isolated  $\text{Fe}^{3+}$  sites; for tetrahe-

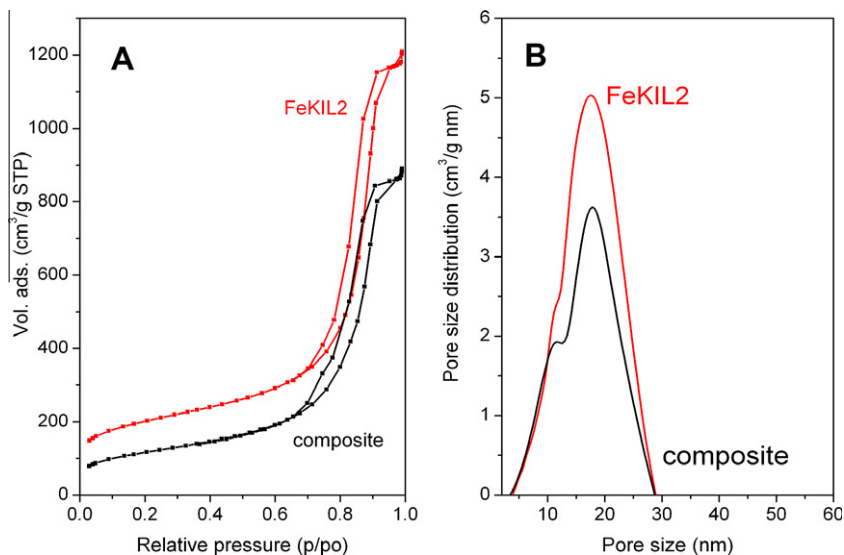


Fig. 4. (A) Nitrogen sorption isotherms and (B) pore size distributions of the mesoporous FeKIL2 and the composite CaCl<sub>2</sub>-FeKIL2.

Table 1

Textural properties of the mesoporous FeKIL2 and the composite CaCl<sub>2</sub>-FeKIL2 before and after the cycling test.

Sample	$S_{\text{BET}}$ (m <sup>2</sup> /g)	$V_t$ (cm <sup>3</sup> /g)	$V_{\text{me}}$ (cm <sup>3</sup> /g)	$V_{\text{mi}}$ (cm <sup>3</sup> /g)	$S_{\text{ex}}$ (m <sup>2</sup> /g)	$S_{\text{me}}$ (m <sup>2</sup> /g)	$w_{\text{BJH}}$ (nm)
<i>Before cycling test</i>							
FeKIL2	712	1.806	1.656	0.081	46	452	17.6
CaCl <sub>2</sub> -FeKIL2	418	1.312	1.286	–	28	347	11.7, 17.9
<i>After cycling test</i>							
FeKIL2	606	1.764	1.634	0.036	62	446	18.3
CaCl <sub>2</sub> -FeKIL2	376	1.094	1.044	–	33	316	11.0, 20.4

Abbreviations:  $S_{\text{BET}}$ , the BET surface area;  $V_t$ , total pore volume evaluated from adsorption isotherm at the relative pressure 0.96;  $V_{\text{me}}$ , primary mesopore volume;  $V_{\text{mi}}$ , micropore volume evaluated by  $\alpha_s$ -method;  $S_{\text{ex}}$ , external surface area evaluated by  $\alpha_s$ -method;  $S_{\text{me}}$ , mesoporous surface area evaluated by  $\alpha_s$ -method;  $w_{\text{BJH}}$ , calculated pore diameter using BJH method.

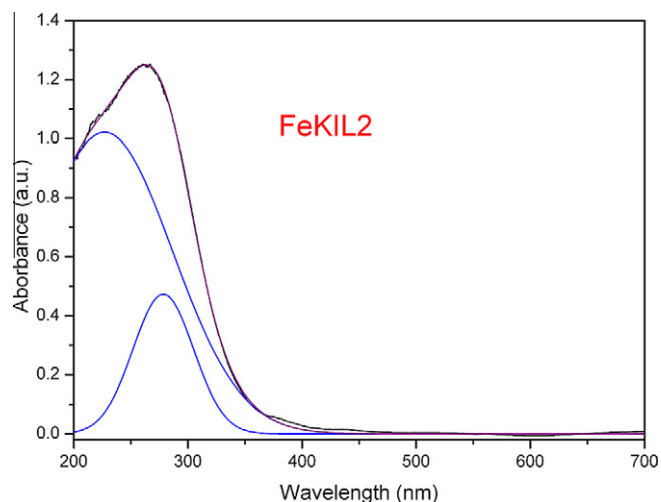


Fig. 5. DRS UV-Vis spectrum of the FeKIL2 matrix (black line – measured spectrum, purple line – fitted spectrum, blue line – deconvoluted sub-bands). (For interpretation of the references to colour in this figure legend, the reader is referred to the web version of this article.)

dral Fe<sup>3+</sup> in framework positions of iron silicalite they are observed at 215 and 240 nm, while for isolated Fe<sup>3+</sup> in octahedral symmetry between 250 and 300 nm [32,34]. Similar observations were found in wormlike mesoporous materials [35].

The UV-Vis spectrum (Fig. 5) of FeKIL2 reveals two peaks at 227 nm and at 278 nm. These bands are assigned to the charge transfer between the Fe and O atoms of Fe–O–Si in the network, indicating the presence of tetrahedrally and octahedrally coordinated Fe(III) species [34]. The incorporation of isolated Fe<sup>3+</sup> ions in the KIL silica network yields active sites [6,34] (structural and/or terminal –OH groups), which can contribute to specific adsorption sites for water. It can also be concluded that Fe<sub>2</sub>O<sub>3</sub> nanoparticles are not present in the FeKIL2 matrix.

### 3.2. Water sorption characterization

For a first estimation of the water capacity [6] for the mesoporous FeKIL2 and the composite, the samples were stored in high humidity atmosphere (75% at 25 °C) and subsequently subjected to TG analysis. Fig. 6 shows TG and DTG curves of both materials. Water is desorbed up to 120 °C due to physically bonded water molecules in the mesostructure. DTG curves evidence one adsorption site for water molecules for both samples, probably in the mesopores. The water loss up to 150 °C for FeKIL2 is 18.8%, while the composite shows a loss of 42.2%. The water capacity, determined by dividing the weight loss due to water desorption with the weight of the sorbent [6] at 150 °C as the reference mass, is 0.23 g/g for the matrix and 0.73 g/g for the composite. Out of these non-equilibrium measurements it can be concluded that the presence of CaCl<sub>2</sub> in the composite increase the amount of water in the sorbent.

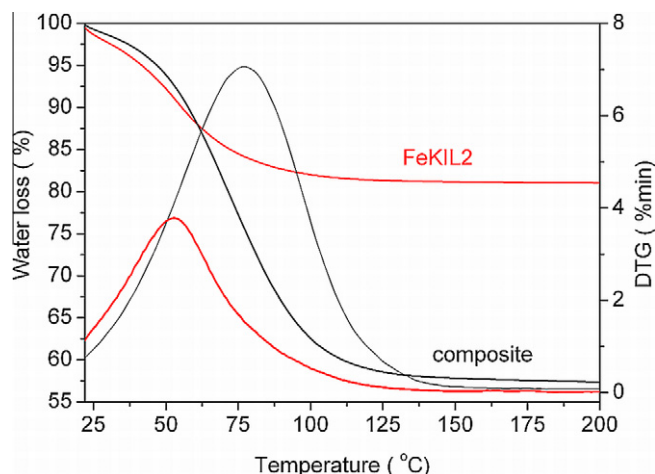


Fig. 6. TG and DTG curves of the FeKIL2 and the composite  $\text{CaCl}_2$ -FeKIL2.

As the above mentioned measurements only give a first estimation on the possible water capacity, detailed equilibrium measurements under defined humidity conditions were performed. The water sorption uptake curves of the FeKIL2 matrix and the composite in Fig. 7 show typical characteristics of the mesoporous hydrophilic adsorbents. The adsorption isobars at 1.2 and 5.6 kPa, respectively, show a nearly linear uptake up to a relative pressure of 0.5, with an increase at higher relative pressure. The water sorption capacity of the composite is improved due to the presence of  $\text{CaCl}_2$ , which interacts with water [9]. The composite shows a maximum water uptake of 0.58 g/g under the given conditions. The difference to the above given maximum uptake is probably due to slow adsorption dynamics and therefore non-equilibrium, although isothermal hold time for the last adsorption point was more than 10 h in the TG-DSC measurement. The matrix shows an uptake of 0.21 g/g, which is in good agreement to the results of TG measurements.

With regard to a sorption heat storage application the important property is the possible loading lift within the thermodynamic cycle. Depending on the boundary conditions, a possible loading lift for the composite is approximately 0.20 g/g as illustrated in Fig. 8. Here, the working conditions are a maximum desorption temperature of 150 °C at 5.6 kPa condenser pressures and a very low minimum adsorption temperature of 25 °C at 1.2 kPa evapora-

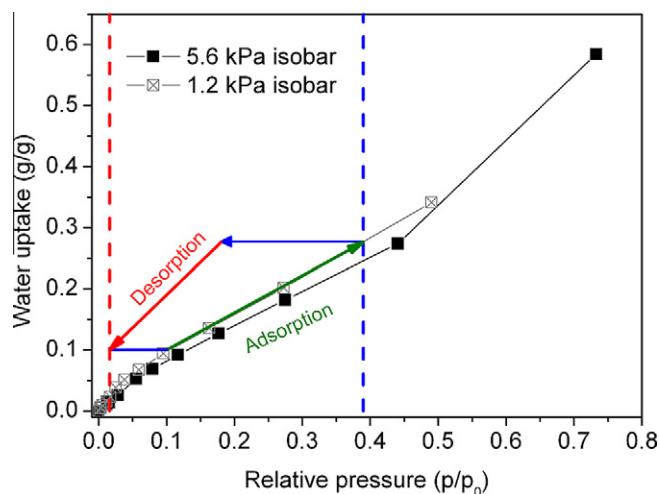


Fig. 8. Thermodynamic cycle of the composite  $\text{CaCl}_2$ -FeKIL2. The maximum working range of a typical sorption heat storage cycle is indicated by perpendicular lines.

tor pressures. These are typical temperatures for heat transformation application, as e.g. 5.6 kPa condenser pressures corresponds to a condensing temperature of 35 °C. This temperature can either be reached for heat rejection devices in summer or for direct heating in winter. The evaporator pressure of 1.2 kPa corresponds to an evaporation temperature of 10 °C, which is either a good value for low temperature heat source in winter or a good value for a cooling application in summer. It has to be mentioned, that the minimum adsorption temperature of 25 °C is slightly too low for direct heating purposes, however, this marks a maximum working windows. The heat of adsorption for the high energy sites has been determined to be 55.2 kJ/mol, whereas the major part of the adsorption takes place with a heat of adsorption of 50.4 kJ/mol, which is approx. 8% higher than the evaporation enthalpy of water and 10% higher than the heat of adsorption of silica gel- $\text{CaCl}_2$  composite, containing 40% of the salt [36]. Therefore, the heat storage capacity under the above given conditions can roughly be estimated to 560 kJ/kg of the composite material.

Beside the loading lift within the cycle and the possible heat of adsorption, the repeated hydrothermal stability is the third important value with regard to a cyclic adsorption process for heat storage applications [37]. Although the leakage of the salt is mentioned

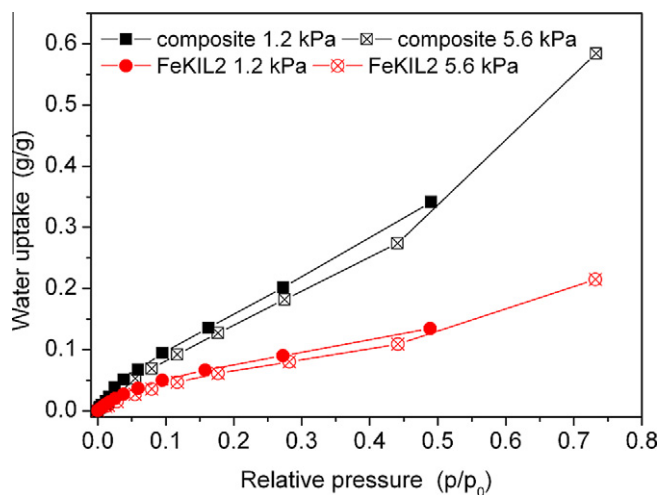


Fig. 7. Water sorption isobars at 1.2 and 5.6 kPa, displayed versus the relative pressure thus giving an isothermal representation of mesoporous FeKIL2 and the composite  $\text{CaCl}_2$ -FeKIL2.

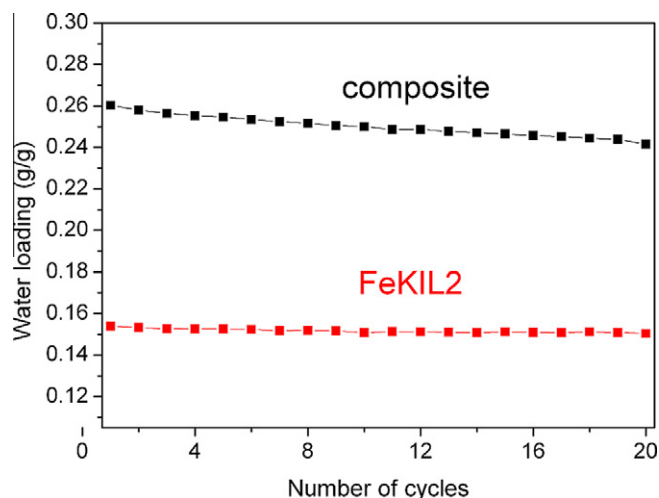


Fig. 9. Hydrothermal treatment of 20 cycles between temperatures of 150 °C and 40 °C at a water vapour pressure of 5.6 kPa.

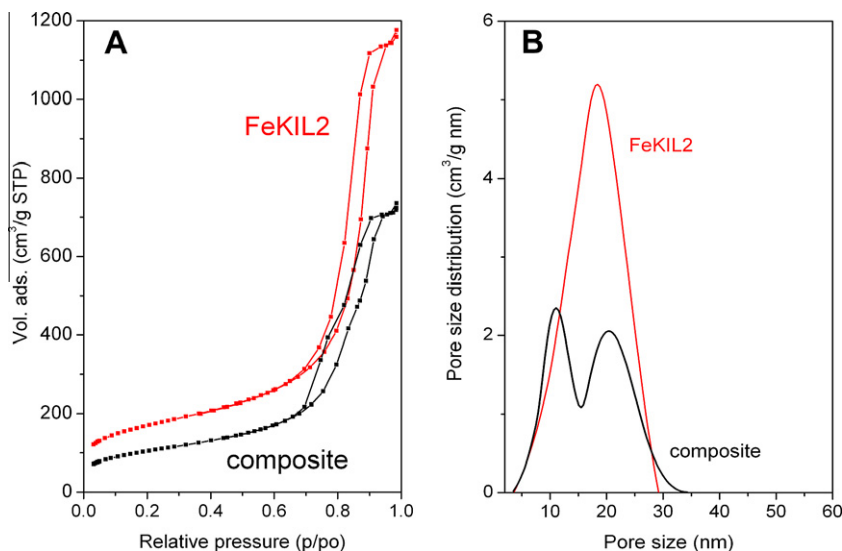


Fig. 10. (A) Nitrogen sorption isotherms and (B) pore size distributions of FeKIL2 and the composite  $\text{CaCl}_2$ -FeKIL2 after the cycling test.

as a possible problem [18], the repeated hydrothermal treatment was, to the best of our knowledge, not performed so far on comparable composites.

To evaluate the hydrothermal stability of the composite, the sample has been exposed to a short-cycle hydrothermal treatment consisting of 20 cycles between temperatures of 150 and 40 °C at a water vapour pressure of 5.6 kPa. In the following step, the water uptake for each cycle between 150 and 40 °C has been determined as a first benchmark. As it can be seen in Fig. 9, there is only a small loss of water uptake capacity in FeKIL2 (0.6%) and in the composite (3.6%), which confirms the comparatively good initial hydrothermal stability of FeKIL2 and the composite under the operating conditions. However, the composite shows a continuous, nearly linear degradation, which may result in a significant decrease of the capacity after hundreds of cycles.

Nevertheless, the porous structures of the FeKIL2 and the composite maintain after the cycling test, as determined by nitrogen adsorption isotherms. Nitrogen adsorption isotherms for FeKIL2 and  $\text{CaCl}_2$ -FeKIL2 after the cycling test are shown in Fig. 10A, whereas structural parameters determined on the basis of these isotherms are listed in Table 1. The sorption isotherm of FeKIL2 is very similar to that of FeKIL2 sample before the cycling test. Adsorption and desorption branches are still almost vertical and nearly parallel, showing the material with uniformly sized pores in a narrow pressure range. This result confirms that FeKIL2 is hydrothermally stable porous matrix. On the other hand, the shape of the isotherm of the composite is significantly changed. The isotherm is less intense and the hysteresis loop is widening. The two step desorption is present, showing that  $\text{CaCl}_2$  nanoparticles are still present in the mesopores of the matrix.

After the cycling test two PSD maxima of the composite become more resolved representing the open mesopores and the narrowed pores (Fig. 10B). As it can be observed, the maximum of the open mesopores of the composite shifts to higher pore size (20.4 nm) [32], is less intense and becomes broader. At the same time, the maximum for narrowed mesopores shifts to lower pore diameter (11 nm). Specific surface areas of the composites before and after the short-cycle hydrothermal treatment remain similar. The total pore and mesopore volume were decreased after the cycling test. No leaching of  $\text{CaCl}_2$  was directly observed after the cycling test, as it is usually observed for these materials [18]. It can be concluded that the FeKIL2 matrix can prevent in a first stage  $\text{CaCl}_2$  leaching from the mesopores of the matrix. The composite  $\text{CaCl}_2$ -

FeKIL2 shows a promising hydrothermal stability for the first 20 cycles between temperatures of 150 and 40 °C at water vapour pressure of 5.6 kPa.

#### 4. Conclusions

New composite  $\text{CaCl}_2$ -FeKIL2 is the material with potential applications as water sorbent for thermo-chemical heat storage. The mesopores of FeKIL2 matrix are formed by the aggregation of iron silicate nanoparticles, which create the network with interparticle voids. UV-Vis spectroscopy reveals that ferric ions are tetrahedrally and octahedrally coordinated, confirming the incorporation of iron in the silica KIL2 network. The presence of  $\text{CaCl}_2$  in FeKIL2 matrix is evidenced from  $\text{N}_2$ -sorption isotherms.  $\text{CaCl}_2$  nanoparticles have been dispersed inside of FeKIL2 mesopores, resulting in the decrease of mesopore diameter of narrowed pores in the composite. The introduction of  $\text{CaCl}_2$  in the FeKIL2 matrix improves the maximum water sorption capacity for approximately 3 times, which makes the composite a potential water sorbent material for low temperature heat storage. Desorption of water from the composite can be achieved at 120 °C. The repeated hydrothermal stability of  $\text{CaCl}_2$ -FeKIL2 is evaluated for the first time showing that this two-component sorbent is comparatively good hydrothermally stable after 20 cycles between temperatures of 150 and 40 °C at water vapour pressure of 5.6 kPa.

#### Acknowledgement

We thank for the support to the Slovenian Research Agency through the research program P1-0021-0104 and research projects J1-3604 and Z1-9144. The work is also a part of the IEA joint network »Compact Thermal Energy Storage Material Development for System Integration«. We thank Dr. Matjaž Mazaj (National Institute of Chemistry Slovenia) for providing TEM pictures and Harry Kummer (Fraunhofer Institute for Solar Energy Systems) for cycling test measurements.

#### References

- [1] H. Stach, J. Mugele, J. Jänchen, E. Weiler, *Adsorption* 11 (2005) 393–403.
- [2] A. Ristić, N. Zabukovec Logar, S.K. Henninger, V. Kaučič, *Adv. Funct. Mater.* 22 (2012) 1952–1957.
- [3] Yu.I. Aristov, doi:10.1016/j.applthermaleng.2011.09.003.

- [4] A. Hauer, in: H.O. Paksoy (Ed.), *Thermal Energy Storage for Sustainable Energy Consumption*, Springer, 2007, pp. 393–408.
- [5] K.E. N'Tsoukpoe, H. Lui, N.L. Pierres, L. Luo, *Renew. Sust. Energ. Rev.* 13 (2009) 2385–2396.
- [6] E.P. Ng, S. Mintova, *Microporous Mesoporous Mater.* 114 (2008) 1–26.
- [7] H.T. Chua, K.C. Ng, A. Chakraborty, N.M. Oo, M.A. Othman, *J. Chem. Eng. Data* 47 (2002) 1177–1181.
- [8] J.S. Oh, W.G. Shim, J.W. Lee, J.H. Kim, H. Moon, G. Seo, *J. Chem. Eng. Data* 48 (2003) 1458–1462.
- [9] Yu.I. Aristov, *J. Eng. Therm.* 16 (2007) 63–72.
- [10] I.A. Simonova, A. Freni, G. Restuccia, Yu.I. Aristov, *Microporous Mesoporous Mater.* 122 (2009) 223–228.
- [11] L.G. Gordeeva, A.D. Grekova, T.A. Krieger, Yu.I. Aristov, *Microporous Mesoporous Mater.* 126 (2009) 262–267.
- [12] L.G. Gordeeva, E.V. Savchenko, I.S. Glaznev, V.V. Malakhov, Yu.I. Aristov, *J. Colloid Interface Sci.* 301 (2006) 685–691.
- [13] G. Restuccia, G. Cacciola, Yu.I. Aristov, *React. Kinet. Catal. Lett.* 63 (1998) 81–88.
- [14] M.M. Tokarev, L.G. Gordeeva, V. Romannikov, I. Glaznev, Yu.I. Aristov, *Int. J. Thermal Sci.* 41 (2002) 470–474.
- [15] I.V. Ponomarenko, I. Glaznev, A.V. Gubar, Yu.I. Aristov, S.D. Kirik, *Microporous Mesoporous Mater.* 129 (2010) 243–250.
- [16] I. Glaznev, I. Ponomarenko, S. Kirik, Yu. Aristov, *Int. J. Refrig.* 34 (2011) 1244–1250.
- [17] J. Jänchen, D. Ackermann, E. Weiler, H. Stach, W. Brösicke, *Thermochim. Acta* 434 (2005) 37–41.
- [18] P. Gantenbein, T. Nunez, D. Jaehnig, H. Kerskes, H.M. Henning, C. Bales, in: J.Ch. Hadorn (Ed.), *Thermal Energy Storage for Solar and Low Energy Buildings*, IEA-SHC, 2005, p. 121.
- [19] N. Novak Tušar, A. Ristić, G. Mali, M. Mazaj, I. Arčon, D. Arčon, V. Kaučič, N. Zabukovec Logar, *Chem. Eur. J.* 16 (2010) 5783–5793.
- [20] S. Brunauer, P.H. Emmett, E. Teller, *J. Am. Chem. Soc.* 60 (1938) 309–319.
- [21] A. Sayari, P. Liu, M. Kruk, M. Jaroniec, *Chem. Mater.* 9 (1997) 2499–2506.
- [22] M. Kruk, M. Jaroniec, C.H. Ko, R. Ryoo, *Chem. Mater.* 12 (2000) 1961–1968.
- [23] B. Tan, H.J. Lehmler, S.M. Vyas, B.L. Knutson, S.E. Rankin, *Nanotechnology* 16 (2005) 502–507.
- [24] E.P. Barrett, L.G. Joyner, P.P. Halenda, *J. Am. Chem. Soc.* 73 (1951) 373–380.
- [25] S.K. Henninger, F.P. Schmidt, H.M. Henning, *Appl. Therm. Eng.* 30 (2010) 1692–1703.
- [26] M. Kruk, M. Jaroniec, S.H. Joo, R. Ryoo, *J. Phys. Chem. B* 107 (2003) 2205–2213.
- [27] M. Mazaj, W.J.J. Stevens, N.Z. Logar, A. Ristić, N.N. Tušar, I. Arčon, N. Daneu, V. Meynen, P. Cool, E.F. Vansant, V. Kaučič, *Microporous Mesoporous Mater.* 117 (2009) 458–465.
- [28] V. Meynen, P. Cool, E.F. Vansant, P. Kortunov, F. Grinberg, J. Karger, M. Martens, O.I. Lebedev, G. Van Tendeloo, *Microporous Mesoporous Mater.* 99 (2007) 14–22.
- [29] M. Tasbihi, U. Lavrenčič Štangar, A. Sever Škapin, A. Ristić, V. Kaučič, N. Novak Tušar, *J. Photoch. Photobio. A* 216 (2010) 167–178.
- [30] W.W. Lukens, P. Schmidt-Winkel, D. Zhao, J. Feng, G.D. Stucky, *Langmuir* 15 (1999) 5403–5409.
- [31] P.T. Tanev, L.T. Vlaev, *J. Colloid Interface Sci.* 160 (1993) 110–116.
- [32] J. Pérez-Ramírez, M.S. Kumar, A. Brückner, *J. Catal.* 223 (2004) 13–27.
- [33] S. Bordiga, R. Buzzoni, F. Geobaldo, C. Lamberti, E. Giamello, A. Zecchina, G. Leofanti, G. Petrini, G. Tozzola, G. Vlaic, *J. Catal.* 158 (1996) 486–501.
- [34] A. Ristić, K. Lázár, H. Solt, V. Kaučič, *CrystEngComm* 13 (2011) 1946–1952.
- [35] M.S. Hamdy, G. Mul, J.C. Jansen, A. Ebaid, Z. Shan, A.R. Overweg, *Th. Maschmeyer, Catal. Today* 100 (2005) 255–260.
- [36] J. Jänchen, D. Ackermann, H. Stach, W. Brösicke, *Sol. Energy* 76 (2004) 339–344.
- [37] S.K. Henninger, G. Munz, K.F. Ratusch, P. Schossig, *Renewable Energy* 36 (2011) 3043–3049.